Mineralium Deposita (2018) 53:855–870
https://doi.org/10.1007/s00126-017-0787-8

ARTICLE

Geochemical contrasts between Late Triassic ore-bearing and barren intrusions in the Weibao Cu–Pb–Zn deposit, East Kunlun Mountains, NW China: constraints from accessory minerals (zircon and apatite)

Shihua Zhong[1,2] · Chengyou Feng[1] · Reimar Seltmann[2] · Daxin Li[1] · Zhihui Dai[3]

Received: 27 April 2017 / Accepted: 10 December 2017 / Published online: 28 December 2017

Abstract

The Weibao copper–lead–zinc skarn deposit is located in the northern East Kunlun terrane, NW China. Igneous intrusions in this deposit consist of barren diorite porphyry (U–Pb zircon age of 232.0 ± 2.0 Ma) and ore-bearing quartz diorite and pyroxene diorite (U–Pb zircon ages of 223.3 ± 1.5 and 224.6 ± 2.9 Ma, respectively). Whole-rock major and trace element and accessory mineral (zircon and apatite) composition from these intrusions are studied to examine the different geochemical characteristics of ore-bearing and barren intrusions. Compared to the barren diorite porphyry, the ore-bearing intrusions have higher Ce^{4+}/Ce^{3+} ratios of zircon and lower Mn contents of apatite, indicating higher oxidation state. Besides, apatite from the ore-bearing intrusions shows higher Cl contents and lower F/Cl ratios. These characteristics collectively suggest the higher productivity of ore-bearing quartz diorite and pyroxene diorite. When compared with ore-bearing intrusions from global porphyry Cu deposits, those from Cu–Pb–Zn skarn deposits display lower Ce^{4+}/Ce^{3+} and Eu_N/Eu_N^* ratios of zircon and lower Cl and higher F/Cl ratios of apatite. We conclude that these differences reflect a general geochemical feature, and that zircon and apatite composition is a sensitive tool to infer economic potential of magmas and the resulting mineralization types in intrusion-related exploration targets.

Keywords Ce^{4+}/Ce^{3+} · Zircon · Apatite · Skarn deposits · Porphyry deposits · East Kunlun

Introduction

Zircon and apatite are widespread accessory minerals in intermediate to felsic igneous rocks and are resistant to hydrothermal alteration and physical and chemical weathering (Uher et al. 1998; Uher and Cerny 1998; Belousova et al. 2001, 2002a, b; Ballard et al. 2002; Belousova 2006; Mao et al. 2016). During the last decade, a large number of studies have illustrated that the composition of zircon and apatite can well reflect information of their host rocks (Uher et al. 1998; Belousova et al. 2002a, b; Breiter and Skoda 2012; Burnham and Berry 2012; Cao et al. 2012; Seifert et al. 2012; Trail et al. 2012; Bruand et al. 2017) and may be effective as indicator minerals in porphyry exploration (Ballard et al. 2002; Liang et al. 2006; Li et al. 2012; Han et al. 2013; Qiu et al. 2013; Zhang et al. 2013; Zhang et al. 2017). The origin and evolution of ore-forming magmas of skarn deposits are, in many aspects, similar to those of porphyry deposits (Sillitoe and Bonham 1990; Baker et al. 2004; Meinert et al. 2005; Mao et al. 2006; Sillitoe 2010), which means that zircon and apatite may also be applied to exploration of skarn deposits.

The Qimantagh metallogenic belt (QMB), located in the East Kunlun Mountains, NW China, is one of the most important and promising exploration areas for porphyry-/skarn-related Cu–Pb–Zn–Fe deposits in China (Fig. 1a) (Feng et al.

Editorial handling: R. Hu

Electronic supplementary material The online version of this article (https://doi.org/10.1007/s00126-017-0787-8) contains supplementary material, which is available to authorized users.

✉ Shihua Zhong
zhongshihua0703@cags.ac.cn

✉ Chengyou Feng
fengchy@cags.ac.cn

[1] MLR Key Laboratory of Metallogeny and Mineral Assessment, Institute of Mineral Resources, Chinese Academy of Geological Sciences, Beijing 100037, China

[2] Center for Russian and Central EurAsian Mineral Studies, Department of Earth Sciences, Natural History Museum, London SW7 5BD, UK

[3] State Key Laboratory of Ore Deposit Geochemistry, Institute of Geochemistry, Chinese Academy of Sciences, Guiyang 550081, China

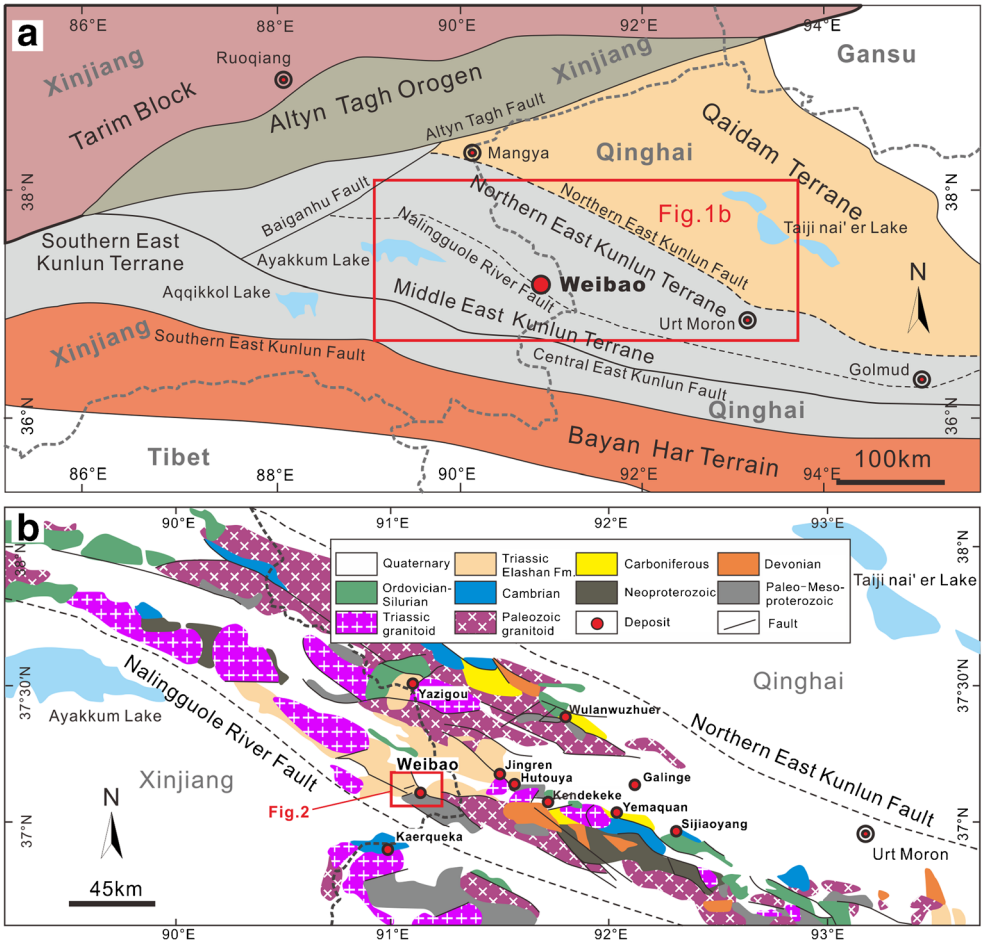

Fig. 1 **a** Simplified geological map of the Qimantagh area and its adjacent districts (modified after Zhong et al. 2017a; and references therein). **b** Geological map of the northern Qimantagh magmatic arc showing the locations of main skarn and porphyry deposits/prospects (modified after Feng et al. 2011; Fang 2015; and Zhong et al. 2017a)

2010, 2012; Zhao et al. 2013), with occurrence of many medium- to large-scale skarn deposits, such as the Weibao Cu–Pb–Zn deposit (Gao et al. 2014b; Zhong et al. 2017a), the Hutouya Cu–Pb–Zn deposit (Feng et al. 2011; Qu et al. 2015), the Galinge Fe deposit (Yu et al. 2015), and the Yemaquan Fe deposit (Gao et al. 2014a). There is a consensus that mineralization is mainly related to Middle to Late Triassic granitoids that are widespread in the QMB (Feng et al. 2012). Nevertheless, published studies also showed that not all Middle to Late Triassic intrusions occurring in the QMB were ore-bearing. Understanding the distinct geochemical patterns between ore-bearing and barren intrusions in the QMB is very important since it can enhance the knowledge about the role of magmas in the formation of those deposits and provide useful information for mineral exploration in this area. So far, few studies have exclusively examined the geochemical differences between Middle to Late Triassic ore-bearing and sub-productive and barren intrusions in the QMB.

The Weibao Cu–Pb–Zn deposit is typical of skarn exploration targets in the QMB, with the igneous intrusions occurring in this deposit being texturally and mineralogically similar to those in other skarn deposits of the QMB. In this study, the major and/or trace element composition of zircon and apatite from three Late Triassic igneous rock units in the Weibao deposit is examined using electron microprobe analysis (EMPA) and laser ablation inductively coupled plasma-mass spectrometry (LA-ICP-MS). Whole-rock geochemical and geochronological data of these intrusions are also presented. Combined with previously published data, we attempt to (1) define the temporal constraints on the sequence of Late Triassic igneous rocks in the QMB and (2) examine the different geochemical characteristics of ore-bearing and barren magmas in the Weibao deposit. Besides, by comparing zircon and apatite composition of Cu–Pb–Zn skarn deposits with that of porphyry Cu deposits, we try to evaluate the application of zircon and apatite as indicator minerals in mineral exploration.

Geological setting

Geology of the QMB and the Weibao deposit

The QMB in the East Kunlun Mountains, NW China, is a Phanerozoic Fe–Cu–Pb–Zn (–Ag) skarn belt that extends for about 550 km in NW–SE direction (Fig. 1a, b) (Feng et al. 2010). The major skarn deposits include Weibao, Hutouya,

Galinge, Yemaquan, and Kaerqueka (Fig. 1b) (Feng et al. 2011; Gao et al. 2014a; Yu et al. 2015; Zhong et al. 2017a). Porphyry mineralization also occurs in this belt, and typical deposits and prospects include Yazigou, Wulanwuzhuer, and Mohexiala (Li et al. 2008; Xu et al. 2014). The basement of this belt is composed of the Jinshuikou, Xiaomiao, and Binggou Groups of Archean–Proterozoic age. The dominant host rocks for skarn mineralization are the Mesoproterozoic Langyashan Formation, Ordovician–Silurian Qimantagh Group, and minor Carboniferous strata, which are mainly carbonate rocks and mafic–intermediate clastic rocks in composition.

Fault systems widely occur in the QMB. The faults striking west, west–northwest, and northwest are interpreted to be produced before and/or during the skarn mineralization, therefore, usually controlling economic mineralization (Feng et al. 2010). The north- and northeast-striking fault systems are generally post-skarn and post-mineralization, but likely control the emplacement of post-skarn intrusions (Feng et al. 2010). Besides, the earlier fault systems are likely reactivated by subsequent tectonic activities.

Intermediate–felsic intrusions, including (porphyritic) syenogranite, monzogranite, granodiorite, (porphyritic) granite, quartz diorite, and pyroxene diorite, are volumetrically the most abundant igneous rocks in the QMB (Li et al. 2008; Wang et al. 2009; Feng et al. 2011, 2012; Chen et al. 2012). Besides, basalts, andesite, rhyolite, dacite, and mafic dikes also occur (Zhong et al. 2017a). Geochronological data illustrated that these igneous rocks were mainly formed in the Silurian–Devonian and Triassic (Feng et al. 2012; Gao et al. 2014a; Zhou et al. 2016), with the latter being predominant.

The Weibao deposit, located in the west of the QMB, is an intermediate Cu–Pb–Zn–(Ag) skarn deposit, with a total resource of 33 million metric tonnes (Mt) at average grade of 0.15% Cu, 1.01% Pb, 1.22% Zn, and 9.01 g/t Ag. It comprises three ore blocks, known as Weixi, Main, and Weidong from west to east (Fig. 2a). Previous exploration revealed that Cu mineralization primarily occurred at Weixi, whereas the other two ore blocks were mainly characterized by Pb–Zn mineralization (Zhong et al. 2017a). However, based on new data from deep drill holes and geophysical surveys, a great deal of Cu mineralization is also found in the subsurface of Weidong, indicating the similarity between Weixi and Weidong.

In spite of the spatial variations of mineralization, the orebodies in the Weibao deposit are all hosted by the Mesoproterozoic Langyashan Formation that predominantly consists of limestone, marble, skarn, schist, pyroclastic rocks, and minor siltstone (Fig. 2), although minor mineralization can also be found in Middle Devonian basaltic lavas. Spatially, these rocks are unconformably overlain by the Triassic Elashan Formation and underlain by the Paleoproterozoic Baishahe Formation (Fig. 2). The Elashan Formation is mainly composed of andesite, dacite, rhyolite, and pyroclastic rocks, whereas the Baishahe Formation dominantly consists of gneiss, marble, and amphibolite manifesting amphibolite and granulite facies metamorphism. Both the Elashan and Baishahe Formations are nonreactive and do not host significant skarn mineralization. More detailed descriptions about stratigraphy, structure, alteration, and mineralization in the Weibao deposit can be found in Fang (2015) and Zhong et al. (2017a).

Igneous rocks in the Weibao deposit

Based on previous geological mapping and drill intersections, the Weibao deposit is characterized by a wide range of igneous rocks similar to those observed in other skarn and porphyry deposits in the QMB. Quartz diorite (also referred to as granodiorite by Zhou et al. 2015) and pyroxene diorite (also referred to as granite by Fang 2015) are volumetrically the most abundant igneous rocks at Weixi and Weidong, respectively (Fig. 2b, c). Major constituents of quartz diorite are oscillatory zoned plagioclase, hornblende, biotite, magnetite, quartz, and minor pyroxene. Besides, it locally contains macroscopic mafic micro-granular enclaves (MMEs), which are regarded as evidence of magma mixing (Zhou et al. 2015). Pyroxene diorite predominantly consists of oscillatory zoned plagioclase, hornblende, biotite, magnetite, and less quartz and more pyroxene than in quartz diorite. Quartz diorite and pyroxene diorite intruded the host rocks (i.e., the Langyashan Formation; Zhong et al. 2017a) and are believed to have resulted in alteration and mineralization in the Weibao deposit (Fang 2015; Zhou et al. 2015). This is firmly evidenced by an observed alteration (Fig. 3a, c) and disseminated sulfides, e.g., galena (Fig. 3d), sphalerite, chalcopyrite (Fig. 3e), and pyrite (Fig. 3e), in those two intrusions. Diorite porphyry is also relatively abundant in the Weibao deposit and normally intercepted by deep drill holes. It is texturally heterogeneous, and in some interceptions, abruptly transitions to diorite with fine-grained textures. Mineralogically, it contains phenocrysts of oscillatory zoned plagioclase, hornblende, biotite, and minor quartz and pyroxene in a groundmass of plagioclase and biotite. Unlike quartz diorite and pyroxene diorite, no economic mineralization is found in diorite porphyry and it has no recognized genetic relationship to skarn or mineralization in the Weibao deposit, although strong sericitic alteration in diorite porphyry can also be locally observed (Fig. 3b). Crosscutting relationships among these three intrusions are not observed.

Apart from the igneous rocks mentioned above, mafic and aplite dikes are also found in the Weibao deposit (Zhong et al. 2017a). Mafic dikes are observed in the whole mine area (Fig. 2b, c), ranging from several 10 cm to several meters in width. Texturally, they are fine-grained with mafic minerals altered by chlorite, carbonate, and epidote. Aplite dikes, however, mainly crop out at Weixi and are normally fine-grained, moderately porphyritic, up to several meters in width. These

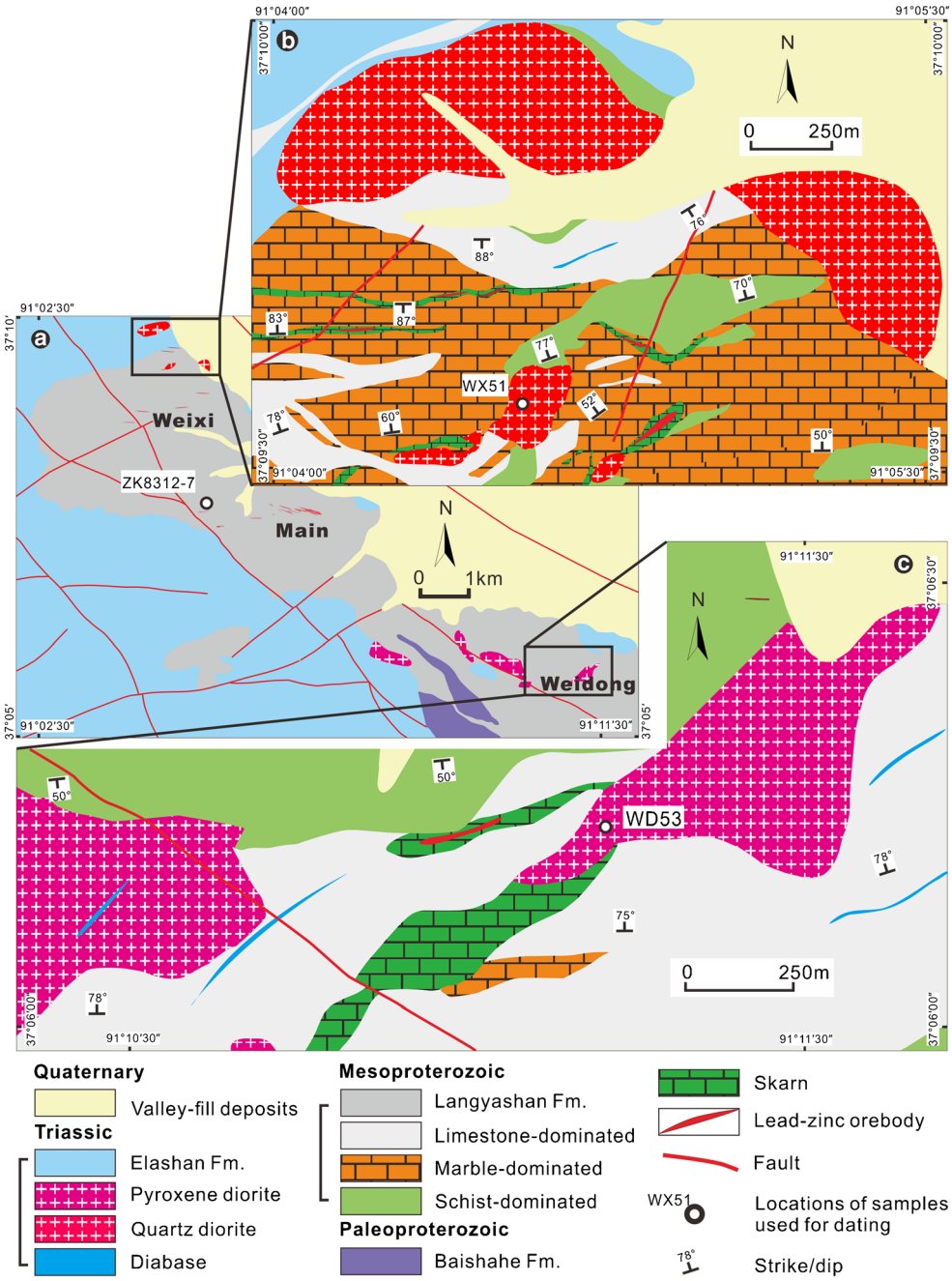

Fig. 2 **a** Simplified geological map of the Weibao district showing locations of Weixi, Main, and Weidong (modified after Zhong et al. 2017a). **b** Geological map of the north Weixi showing the location of quartz diorite. **c** Geological map of Weidong showing the location of pyroxene diorite

rocks are as yet undated but are inferred to be post-skarn because they are observed locally cutting the skarn and orebodies in the Weibao deposit.

Sampling and analytical methods

Sampling

Igneous rocks studied in this work are quartz diorite, pyroxene diorite, and diorite porphyry. The first two igneous rocks are ore-bearing, whereas the diorite porphyry is representative of the barren intrusions in this deposit. More than 50 igneous rock samples were collected. Eight least altered samples were selected for geochronological and/or geochemical analysis based on careful examination under the polarizing microscope. Detailed descriptions of these samples in terms of mineralogy and alteration are listed as an electronic supplementary material (ESM 1: Table S1).

Zircons were separated from three samples, i.e., WX51 (quartz diorite), ZK8312–7 (diorite porphyry), and WD53 (pyroxene diorite), using magnetic and heavy liquid separation. Approximately, 300 zircon grains from each sample were mounted and polished in 25-mm epoxy discs. Unlike zircon,

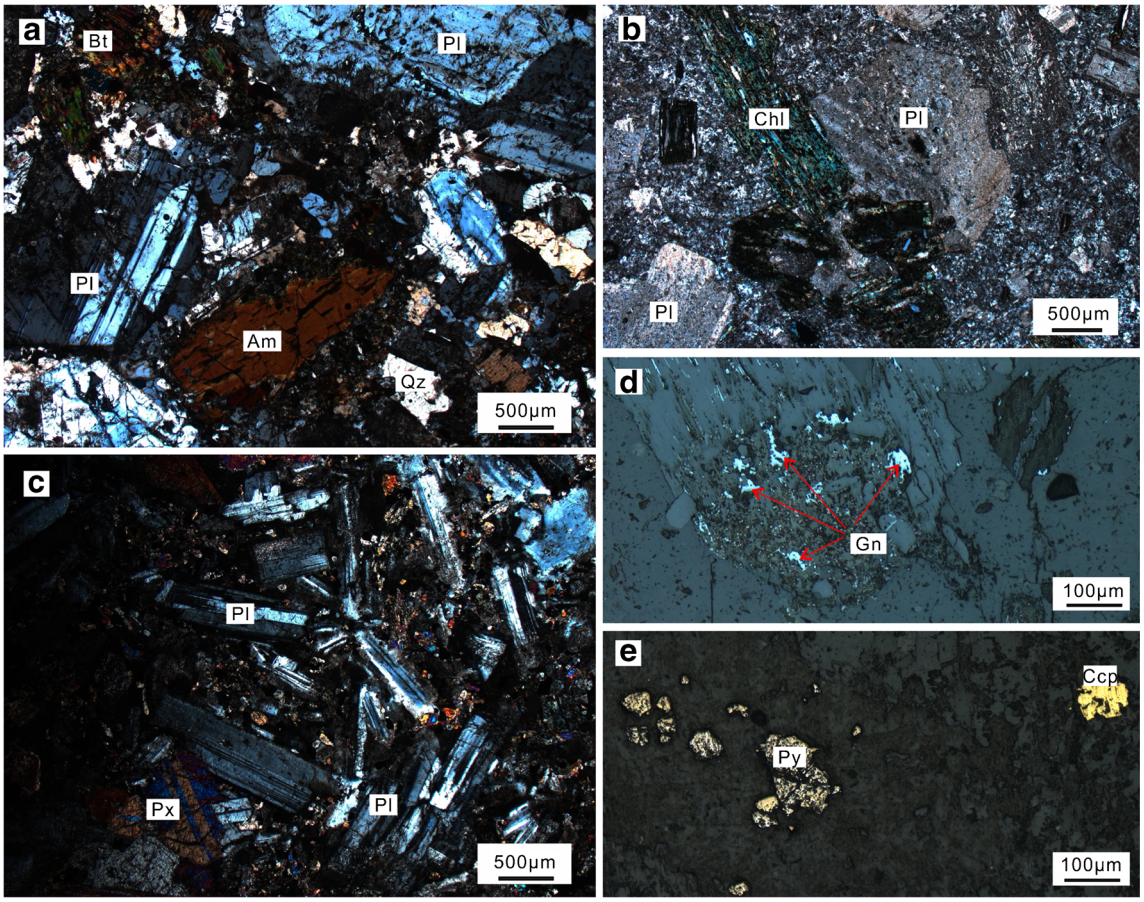

Fig. 3 Photographs of main igneous rocks in the Weibao deposit. **a** Quartz diorite from Weixi with plagioclase altered by sericite and mafic minerals (biotite and amphibole) altered by chlorite (cross-polarized light). **b** Diorite porphyry from Weixi with biotite and plagioclase strongly altered by chlorite and sericite respectively (cross-polarized light). **c** Pyroxene diorite from Weidong with mafic minerals (pyroxene, biotite, and amphibole) altered by sericite and chlorite (cross-polarized light). **d** Galena in quartz diorite (reflected light). **e** Chalcopyrite and pyrite in pyroxene diorite (reflected light). Abbreviations: Am—amphibole, Bt—biotite, Chl—chlorite, Gn—galena, Pl—plagioclase, Px—pyroxene, Py—pyrite, Qz—quartz

apatite grains used in this study were not separated by standard mineral separation techniques; rather, they were selected by employing optical and back-scattered electron (BSE) microscopy in polished thin sections. This approach combines the detailed textural relationships between apatite and the host phases, allowing for a more precise interpretation for apatite composition. For whole-rock major and trace element analysis, about 1 kg of each sample was trimmed to remove weathered surfaces, cleaned with deionized water, crushed and then powdered with an agate mill.

CL images and U–Pb dating

The internal zoning patterns of the zircon crystals were observed by cathodoluminescence (CL) image analysis at the Institute of Mineral Resources, Chinese Academy of Geological Sciences (CAGS), Beijing, China. Using a combination of CL images and optical microscopy, the clearest, least fractured zircon crystals were selected as suitable targets for laser ablation.

In-situ U–Pb analysis for sample WD53 was carried out by the Cameca IMS–1280 secondary ion mass spectrometer (SIMS) at the Institute of Geology and Geophysics, Chinese Academy of Sciences (IGGCAS), Beijing, China, whereas that for samples WX51 and ZK8312–7 was carried out by laser ablation inductively coupled plasma mass spectrometry (LA-ICP-MS) at the State Key Laboratory of Continental Tectonics and Dynamics, CAGS. The beam sizes are of 30 μm diameter for SIMS dating and 35 μm diameter for LA-ICP-MS dating. Instrumental conditions and detailed measurement procedures for SIMS and LA-ICP-MS analysis are the same as those described by Li et al. (2010) and Hou et al. (2009), respectively. Data processing was carried out using the Squid and Isoplot programs of Ludwig (2001) and the measured ^{204}Pb was used for the correction of common lead with the two methods.

Major and trace element analysis of whole-rock

Major and trace element analysis of whole-rock was done at National Research Center of Geo-analysis, CAGS. Major

oxides were analyzed with a wavelength X-ray fluorescence spectrometer (3080E), with FeO and loss-on-ignition analyzed by wet chemical methods. Analytical uncertainties were better than 0.5% for all major elements. Trace elements were analyzed with an X-Series inductively coupled plasma mass spectrometer (ICP-MS; Thermo Fisher, USA). The measurement of error and drift were controlled by regular analysis of standard samples with a periodicity of 10%. Analyzed uncertainties of ICP-MS data at the ppm level were better than 10%.

BSE imaging and major element analysis of apatite

BSE imaging and major element analysis of apatite were performed using electron-probe microanalysis (EPMA) at the Electron Probe Laboratory, CAGS, using a JEOL JXA-8800 instrument with a 2- to 5-μm-diameter beam. F, Na, and Cl were analyzed with a 4-nA beam current and 10-kV accelerating voltage in the first instrumental pass; the remaining elements were measured utilizing a 20-nA beam current and 20-kV accelerating potential in the second instrumental pass. Natural minerals and synthetic oxides were used as standards, and the ZAF software provided by JEOL was used to correct matrix effects. The accuracy of the analytic results is 1–5% depending on the abundance of the element.

Trace element analysis of zircon and apatite

Trace element analysis of zircon and apatite was performed using a LA-ICP-MS at the State Key Laboratory of Ore Deposit Geochemistry, Institute of Geochemistry, Chinese Academy of Sciences (IGCAS), Guiyang, China. Laser sampling was accomplished employing a 193-nm ArF excimer laser connected to an Agilent 7700× quadruple ICP-MS. Laser ablation was operated at a relatively constant frequency of 6 Hz, with the spot diameter of 44 μm for zircons from samples WX51 and ZK8312–7 and of 32 μm for zircons from sample WD53 and apatite from three samples. Each analysis incorporated a background acquisition of approximately 20 s (gas blank) followed by 60 s data acquisition from the sample. The Agilent Chemstation was utilized for the acquisition of each individual analysis. Corrections of zircon data were made for mass bias drift which was evaluated by reference to standard glass NIST 610, and trace-element concentrations were obtained by normalizing count rates for each analyzed element to those for Si, and assuming SiO_2 to be stoichiometric in zircon with a concentration of about 32.8 wt% (Ballard et al. 2002). P and Ca, and K and Th were used in this study to evaluate the possible involvements of mineral inclusions (apatite, K-feldspsar and monazite, respectively); when spiders of these elements are encountered, the analysis was discarded. Besides, the analysis spots showing high P contents (> 1000 ppm) were also discarded even though spiders of P were not observed, since they might be contaminated by even-distributed, micro-metric apatite inclusions.

Trace element contents of apatite were obtained through calibration of relative element sensitivities using the NIST-610, NIST-612, and NIST-614 glass as the external standard, and normalization of each analysis to the electron microprobe data for ^{43}Ca as an internal standard. Where direct electron microprobe data were not available, the median Ca content from other apatite crystals within the same sample was used in the calculation. The preferred values of element concentrations for the USGS reference glasses are from the GeoReM database (http://georem.mpch-mainz.gwdg.de/). Off-line selection and integration of background and analyte signals, and time-drift correction and quantitative calibration were performed by *ICPMSDataCal* (Liu et al. 2008).

Results

Zircon U–Pb age

Zircon crystals from three igneous rock samples display a variety of sizes, morphology, and colors ranging from clear to pale yellow. Typical CL images of zircon are shown in ESM 2; U–Pb dating data are summarized in ESM 1 (Table S2).

Diorite porphyry: Sample ZK8312–7 contains clear to pale, euhedral to subhedral, nearly granular (normally 200 to 400 μm in size) zircons which display concentric zonation patterns under CL (ESM 2). These zircons contain many mineral inclusions, which are predominantly composed of apatite, and to a lesser extent K-feldspar, as indicated by the energy dispersive spectrum analysis. Twenty single grains of zircon were analyzed by LA-ICP-MS, giving a wide range in uranium (147–571 ppm) and thorium (90–778 ppm) contents, as well as Th/U ratios ranging from 0.50 to 1.36 (ESM 1: Table S2). They define a linear array on the concordia diagram (ESM 2) and are anchored by a cluster of concordant analyses, yielding a weighted mean $^{206}Pb/^{238}U$ age of 232.0 ± 2.0 Ma (MSWD = 0.81) (ESM 2). This age likely represents the time of emplacement of diorite porphyry.

Quartz diorite: Most zircons in sample WX51 are pale yellow to light brown, elongated and tabular (150 × 50 to 300 × 150 μm in size); some zircons are granular with a size of < 200 μm (ESM 2). In spite of these discrepancies, they both display systematic zircon growth patterns. The energy-dispersive spectrum analysis manifests that minor apatite and K-feldspar inclusions occur within the studied zircons. Similar to sample ZK8312–7, 20 zircon grains from sample WX51 were analyzed by LA-ICP-MS. These zircon grains display relative uniform U and Th contents, ranging from 215 to 491 ppm and 86 to 283 ppm, respectively (ESM 1: Table S2). Th/U ratios range from 0.39 to 0.62. These zircon

grains give a weighted mean $^{206}Pb/^{238}U$ age of 223.3 ± 1.5 Ma with an MSWD = 0.67 (ESM 2). This age is interpreted to be the age of crystallization of quartz diorite. However, this age is slightly younger than the previously reported SIMS zircon U–Pb age of 227.7 ± 3.1 Ma (MSWD = 2.8) (Zhou et al. 2015). It is possible that the observed age range in this unit reflects a long-lived magma system, rather than only differences in dating methods considering that sampling sites were different in each case (Zhou et al. 2015), and taking into account the batholithic size of the quartz diorite at Weixi. Another interpretation is that the previously obtained age is overestimated considering the probable influence of an older zircon core (ESM 2) and the large MSWD value.

Pyroxene diorite: Zircons from sample WD53 are primarily light brown, subhedral, smaller in size (mostly < 200 μm) and less abundant compared to those from the other two samples (ESM 2). Besides, few mineral inclusions (e.g., apatite and K-feldspar) are observed within the studied zircons. Nevertheless, they also exhibit well-developed concentric growth bands. Ten zircon grains were analyzed by SIMS. For seven zircon grains used for the age calculation, U and Th contents range from 127 to 736 ppm and 65 to 444 ppm, respectively (ESM 1: Table S2). Their Th/U ratios range from 0.44 to 0.76 and the $^{206}Pb/^{238}U$ ages for individual crystals range over 7 m.y. with a calculated mean age of 224.6 ± 2.9 Ma (MSWD = 0.76) (ESM 2). This age represents the best age estimate of pyroxene diorite emplacement. Two grains (spots WD53–2 and WD53–6) with $^{206}Pb/^{238}U$ ages of 403.3 Ma and 392.5 Ma, respectively, and one grain (spot WD53–4) with the Paleoproterozoic $^{206}Pb/^{238}U$ age of 1723.9 Ma are not included in the age calculation. These zircons are interpreted to be xenocrysts, with the former reflecting incorporation of either Devonian volcanic rocks in the Weibao district (Zhong et al. 2017a) or intrusions associated with that magmatic episode, and the latter probably reflecting incorporation of wall rocks (e.g., the Baishahe Formation) in the Weibao district.

Overall, U–Pb ages reported herein demonstrate Late Triassic magmatism in the Weibao deposit, with igneous rock ages broadly ranging from 232 to 224 Ma.

Whole-rock major and trace elements

The results of whole-rock major and trace elements are shown in ESM 1 (Table S3). Two ore-bearing intrusions (quartz diorite and pyroxene diorite) in the Weibao deposit are characterized by low SiO_2 (52.04 to 61.34 wt%) and K_2O (1.77 to 3.02 wt%), and high $^{T}Fe_2O_3$ (7.10 to 9.07 wt%) and MgO (2.76 to 4.12 wt%). The barren diorite porphyry, however, is characterized by much higher SiO_2 (63.01 to 63.22 wt%) and K_2O (4.34 to 4.78 wt%), and lower $^{T}Fe_2O_3$ (3.86 to 3.97 wt%) and MgO (1.03 to 1.05 wt%) compared to the two ore-bearing intrusions. In the SiO_2 vs. K_2O diagram (Fig. 4a), the two ore-bearing intrusions plot in the field of high-K calc-alkaline granitoids, whereas the diorite porphyry plots in the field of shoshonitic rocks. All three intrusions are characterized by light rare earth element (LREE)-enriched patterns, as manifested in the chondrite-normalized rare earth element (REE) diagram (Fig. 4b). The geochemical implications from the whole-rock composition are, however, somewhat compromised by the widespread alteration within these intrusions, as suggested by the high weight loss on ignition (LOI) (1.59–3.51 wt%).

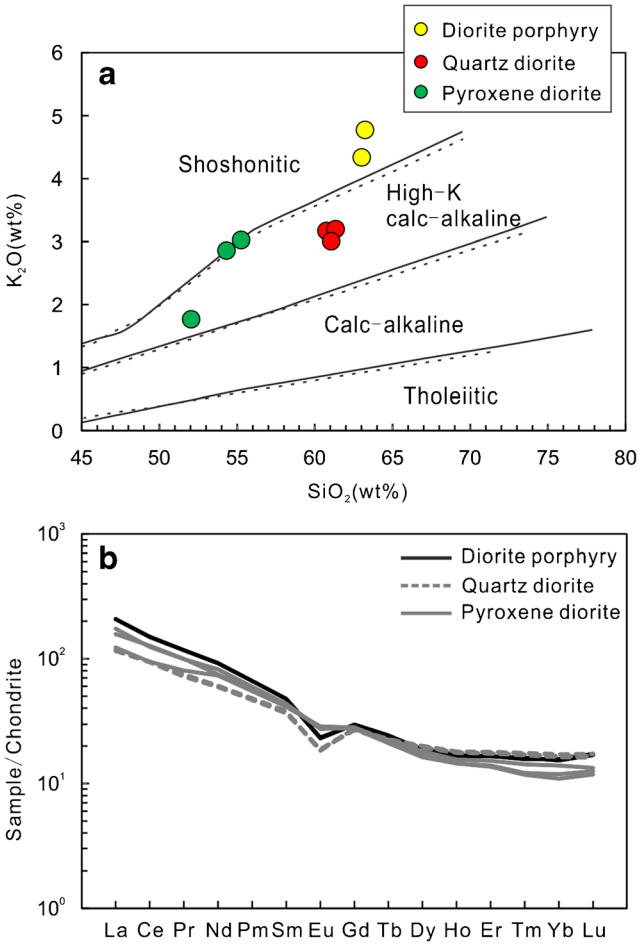

Fig. 4 SiO_2 versus K_2O (**a**) and chondrite-normalized REE (**b**) diagrams of intrusions from the Weibao deposit

Zircon trace elements

Analytical data of trace elements for zircons from the Weibao intrusions are summarized in ESM 3.

ZrO_2 contents in zircons of diorite porphyry (sample ZK8312–7; 58.87 to 66.01 wt%) are lower than the stoichiometric ZrO_2 concentration of ~67.22 wt% in zircons, which might indicate strong cation substitution. In contrast, ZrO_2 contents in zircons of quartz diorite (sample WX51) and pyroxene diorite (sample WD53) are relatively high and can exceed the maximum ZrO_2 concentration of zircon, with

ranges from 63.64 to 68.22 wt% and 60.93 to 69.90 wt%, respectively.

Rb and Sr contents of zircons from three samples are similar and typically less than 10 ppm. Other trace elements in the studied zircons, however, may vary over several orders of magnitude. Th and U contents range from tens of ppm to thousands of ppm, with the highest values in quartz diorite. Hf concentrations are at thousands of ppm, with average values of 7532 ppm for diorite porphyry, 9434 ppm for quartz diorite, and 7523 ppm for pyroxene diorite.

Chondrite-normalized REE abundances for zircons from each rock type are shown in Fig. 5. Chondrite-normalized REE diagrams of zircons from diorite porphyry have some scatter in LREE contents (Fig. 5a). The more elevated LREE contents may represent inherited grains or portions of grains. In contrast, zircons from quartz diorite and pyroxene diorite show consistent and steeply increasing chondrite-normalized REE diagrams from La to Lu with strongly positive Ce anomalies and negative Eu anomalies (Fig. 5b, c). According to the Ce^{4+}/Ce^{3+} calculation method proposed by Ballard et al. (2002) on the basis of a lattice-strain model for mineral-melt partitioning of Ce^{4+} and Ce^{3+} cations, the relationships of Ce and Eu anomalies among different intrusions in the Weibao deposit are examined. Calculated zircon Ce^{4+}/Ce^{3+} and Eu_N/Eu_N^* ratios are listed in ESM 3 (where the subscript indicates chondrite normalization, and $Eu_N^* = (Sm_N \times Gd_N)^{1/2}$). Diorite porphyry shows low Ce^{4+}/Ce^{3+} ratios of zircons, ranging from 2.2 to 15.0 (average: 7.7). In contrast, the two ore-bearing intrusions (quartz diorite and pyroxene diorite) display higher Ce^{4+}/Ce^{3+} ratios, ranging from 12.0 to 280.5 (average: 83.2) and 12.1 to 65 (average: 24.1), respectively. However, the Eu_N/Eu_N^* ratios do not show noticeable differences among the three intrusions in the Weibao deposit, with most values ranging from 0.1 to 0.3. This is clearly manifested by the Eu_N/Eu_N^* versus Ce^{4+}/Ce^{3+} diagram (Fig. 6) in which the two ore-bearing intrusions show much higher Ce^{4+}/Ce^{3+} ratios (> 12) than the barren diorite porphyry, although their Eu_N/Eu_N^* ratios are indistinguishable.

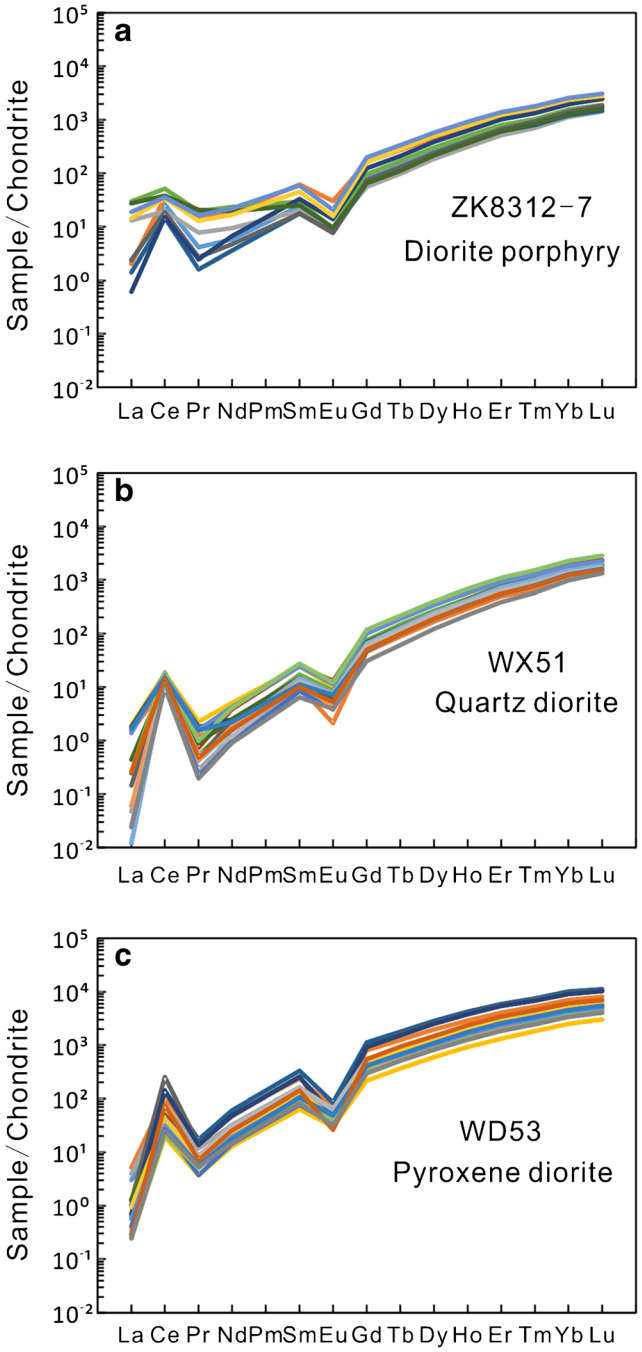

Fig. 5 **a**–**c** Chondrite-normalized REE diagrams of zircons in intrusions from the Weibao deposit

Apatite major and trace elements

Typical BSE images of apatite from the intrusions in the Weibao deposit are shown in Fig. 7. Analytical data of major and trace elements for apatite are summarized in ESM 3 and Fig. 8.

Most apatite grains from the three intrusions in the Weibao deposit are euhedral, and no prominent zonation is observed (Fig. 7). Apatite grains from quartz diorite (sample WX51) and pyroxene diorite (sample WD53) are generally elongated, tabular, 120 × 40 μm to 360 × 50 μm in size (Fig. 7b, c), whereas those from diorite porphyry (sample ZK8312–7) are normally granular and smaller in size (mostly < 40 μm) (Fig. 7). Apatite CaO contents show little variation with increasing whole-rock SiO_2 concentrations (Fig. 8a), whereas P_2O_5 is higher in the mafic end-members (Fig. 8b). Fluorine contents are relatively high (ranging from 1.4 to 2.6 wt%) but indistinguishable between ore-forming and barren intrusions (ESM 3; Fig. 8c). In contrast, chlorine contents are lower and are well distinguished between ore-forming and barren intrusions, with the former displaying higher Cl contents (0.4 to 1.0 wt%) (ESM 3; Fig. 8d). Assuming that F^-, Cl^-, and OH^- fill the anion site, the studied apatite indicates mainly F–OH

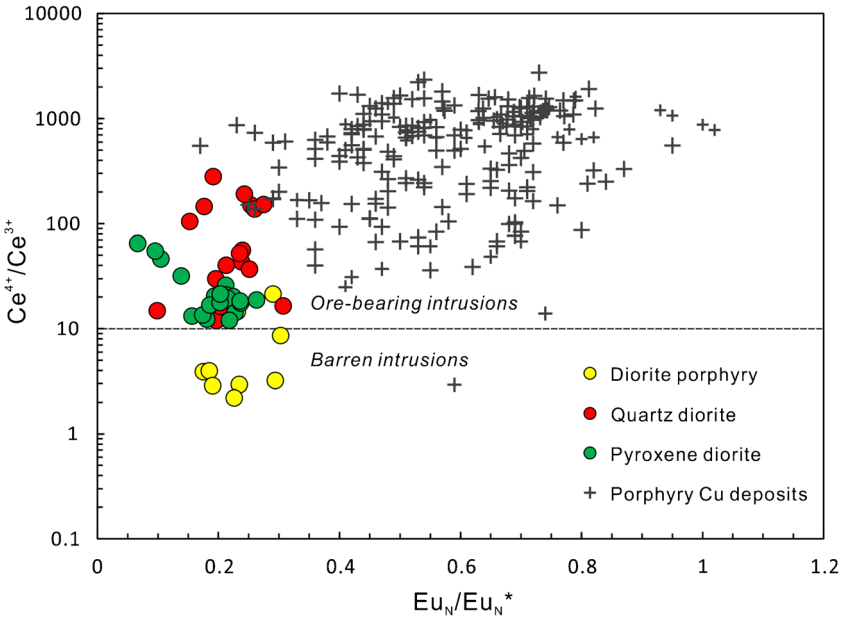

Fig. 6 Zircon Eu_N/Eu_N^* versus Ce^{4+}/Ce^{3+} diagram. Data for porphyry Cu deposits are from the Chuquicamata–El Abra porphyry copper belt (Ballard et al. 2002), the Lower Yangtze River belt (Wang et al. 2013), the Dexin porphyry Cu deposit (Zhang et al. 2013), the Yuhai porphyry Cu deposit (Wang et al. 2017), and the Kalmakyr porphyry Cu–Au deposit (Zhang et al. 2017). All the intrusions are ore-forming except for the diorite porphyry from the Weibao deposit

exchange. Other major elements (Na_2O, MgO, SiO_2, and FeO) in apatite rarely exceed 1 wt% (ESM 3) and are commonly below their detection limits.

V, As, Pb, Th, and U concentrations of the apatite range from less than 1 ppm to tens of ppm and do not show systematic variations between ore-forming and barren intrusions in the Weibao deposit (ESM 3). In contrast, Mn, Sr, and Y contents are much higher, ranging from hundreds of ppm to over several thousand ppm (ESM 3). Besides, Mn concentrations are much higher in diorite porphyry than in the ore-forming intrusions (quartz diorite and pyroxene diorite) (Fig. 8e), although Sr and Y contents do not show systematical variations between ore-forming and barren intrusions (not shown). The studied apatite contains significant amounts of REE substituting for Ca, with total REE concentrations ranging from several thousand ppm to over 1 wt% in both barren and ore-forming intrusions in the Weibao deposit (ESM 3). The high trace element contents, as well as the high F contents, are indicative of the magmatic origin of the studied apatite (Mao et al. 2016; Cao et al. 2012; Patiño et al. 2011; Nash 1984). In the chondrite-normalized REE diagrams (Fig. 9), apatite from the individual intrusions identically displays a negative slope from La to Lu and strong negative Eu anomalies.

Discussion

Geochronology

Zircons from three intrusions in the Weibao Cu–Pb–Zn skarn deposit are predominantly euhedral and display clearly concentric zonation patterns under CL. The U–Pb dates for individual grains are concordant and the Th/U ratios are high (ranging from 0.40 to 1.36 with one exception). All these characteristics advocate that the studied zircons are of magmatic origin and their ages therefore can represent the time of magma emplacement.

The obtained U–Pb ages document multiple magmatic activities in the Weibao deposit. It extends back to ~ 400 Ma, as evidenced by two concordant zircon grains of this age (spot WD53–2, 403.3 Ma; spot WD53–6, 392.5 Ma). This is consistent with our previous study that demonstrated the existence of Devonian magmatic activity in the Weibao deposit (Zhong et al. 2017a). After a very long magmatic lull (~ 160 Ma), igneous activity in the Weibao deposit resumed at about 232 Ma with the emplacement of barren diorite porphyry (232.0 ± 2.0 Ma) at Weixi. The next stage of igneous activity is indicated by ~ 224 Ma zircon U–Pb dates. During this new magmatic cycle, the ore-bearing intrusions were emplaced, which are characterized by quartz diorite at Weixi with the age of 223.3 ± 1.5 Ma and pyroxene diorite at Weidong with the age of 224.6 ± 2.9 Ma. These two ages are indistinguishable when errors are considered, indicating that the ore-bearing magmas were emplaced simultaneously or during a very short time span. As hydrothermal activity and mineralization in porphyry–skarn systems are intimately tied to emplacement of ore-forming intrusions (Razique et al. 2014), the associated hydrothermal and mineralization events in the Weibao deposit probably have similar short durations of just a few million years or less.

At the regional scale, magmatism in the Weibao deposit coincides with that in other porphyry and skarn deposits/prospects in the QMB. For instance, in the Yemaquan Fe skarn deposit the early stage of magmatic activity is characterized by Early to Middle Devonian monzogranite (393 ± 2 Ma; Gao et al. 2014a) and granodiorite (400.8 ± 1.4 Ma to 386 ±

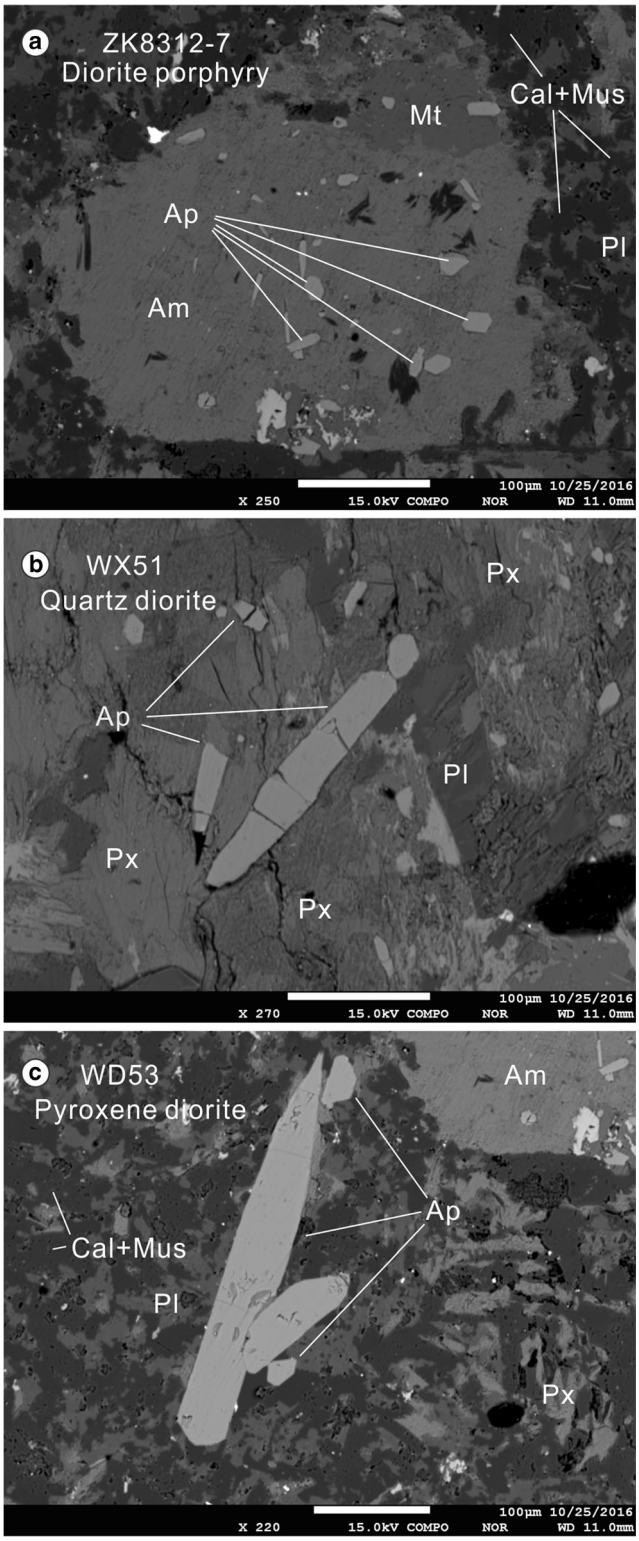

Fig. 7 **a**–**c** Back-scattered electron (BSE) images of typical apatite from the Weibao intrusions. Abbreviations: Ap—apatite, Am—amphibole, Cal—calcite, Pl—plagioclase, Px—pyroxene, Mt—magnetite, Mus—muscovite

1 Ma; Gao et al. 2014a; Qiao et al. 2016), and the late stage of magmatic activity is characterized by porphyritic quartz monzodiorite (219 ± 1 Ma; Gao et al. 2014a), syenogranite (213 ± 1 Ma; Gao et al. 2014a), and granodiorite (220.53 ± 0.69 Ma; Qiao et al. 2016). Similarly, in the Kaerqueka Cu–Pb–Zn skarn deposit, two distinct igneous events were also demonstrated (Wang et al. 2009; Chen et al. 2012; Feng et al. 2012). It should be noted that although Middle to Late Triassic igneous rocks in the QMB are volumetrically comparable to Paleozoic (mainly Early to Middle Devonian) igneous rocks at the regional scale, at the district and deposit scale, however, the former are volumetrically more predominant. Moreover, published molybdenite Re–Os and muscovite $^{40}Ar/^{39}Ar$ dates in these skarn and porphyry deposits gave a similar time span ranging from 224 to 239 Ma (Li et al. 2008; Feng et al. 2011; Yu et al. 2015; and references therein), therefore also indicating that hydrothermal events in the QMB resulted from Triassic magmatic activity. It should be noted that Gao et al. (2014a) argued that both Middle Devonian magmatic activity and Late Triassic magmatic activity were closely related to ore-forming processes in the Hutouya deposit, which might mean two, rather than only one, mineralization events existed in the QMB. However, currently, this assumption still cannot be reliably determined due to lack of direct dating of sulfides and/or hydrothermal minerals in most deposits of the QMB.

Contrasts between ore-bearing and barren intrusions in the Weibao deposit

Magmatic oxygen fugacity

The magmatic oxygen fugacity is a key factor in controlling the magmatic fertility of porphyry deposits (Lehmann 1990; Wittenbrink et al. 2009; Sun et al. 2013, 2015; Zhang et al. 2017; Zhong et al. 2017b). There is a consensus that oxidized magmas are more favorable than reduced magmas in generating porphyry Cu deposits (Imai 2002; Liang et al. 2006; Lu et al. 2016; Li et al. 2017a), considering that at higher oxygen fugacity, magmatic sulfur exists mainly as sulfate (SO_4^{2-}) which has a much higher solubility in silicate melts than sulfide and will tend to delay or even prevent saturation of a magmatic sulfide phase (Ballard et al. 2002; Richards 2003). When it comes to Cu (–Pb–Zn) skarn deposits, this is also applicable because of the similar magmatic origins and evolutions of porphyry and skarn deposits (Li et al. 2017b).

The zircon Eu_N/Eu_N^* and especially Ce^{4+}/Ce^{3+} ratios have been firmly demonstrated to be an effective proxy of the magmatic oxygen fugacity (e.g., Ballard et al. 2002; Liang et al. 2006; Li et al. 2012; Trail et al. 2012; Qiu et al. 2013; Xu et al. 2016; Gardiner et al. 2017). In the Weibao Cu–Pb–Zn skarn deposit, the ore-bearing intrusions display higher zircon Ce^{4+}/Ce^{3+} values (> 12) than those of barren intrusions, although their Eu_N/Eu_N^* ratios are indistinguishable. This indicates that compared to the barren diorite porphyry, the ore-bearing intrusions are much more oxidized and thus more productive for

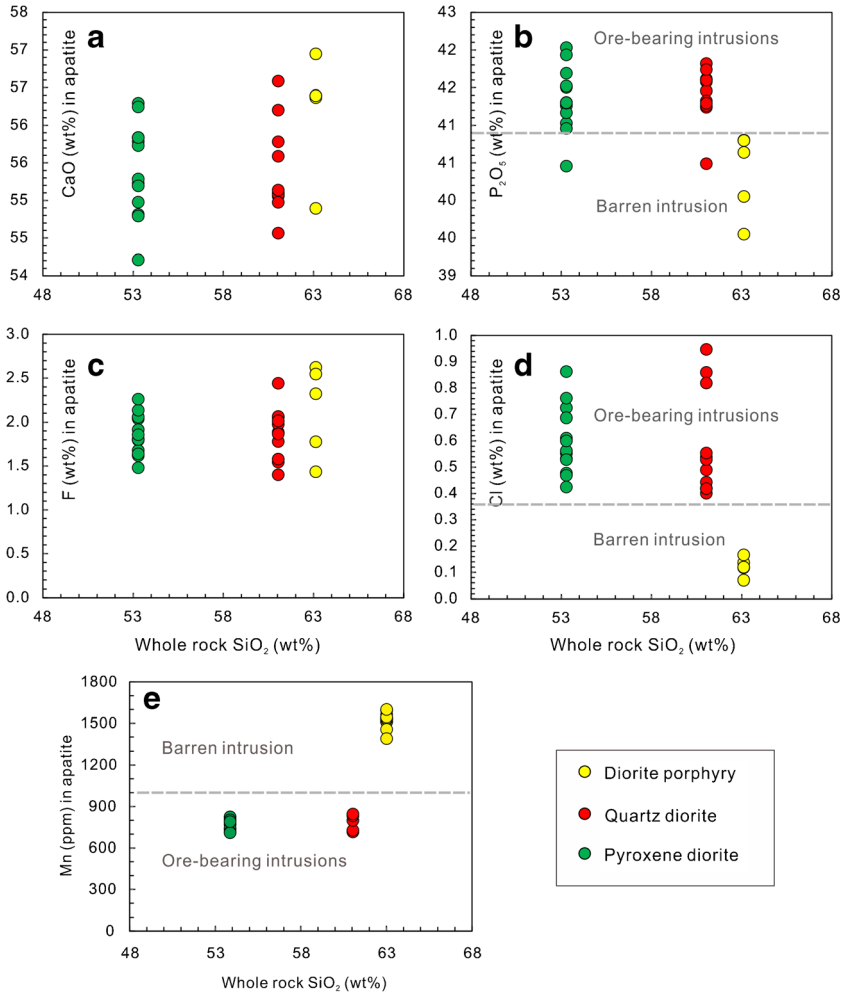

Fig. 8 **a**–**e** Correlation between major and trace elements in apatite and the whole-rock SiO_2 content. Note that whole-rock SiO_2 contents are from the average values of the corresponding intrusions

Cu mineralization. Unlike Cu, Pb and Zn can behave as incompatible elements regardless of the redox state, which means that Pb–Zn mineralization can occur either at high oxygen fugacity or at relatively low oxygen fugacity. This is evidenced by many findings that both S-type (and thus low oxidation state) or I-type (and thus higher oxidation state) granitoids can form Pb–Zn deposits (e.g., Fu et al. 2017; Niu et al. 2017). In other words, the oxidation state is not a controlling factor for Pb–Zn mineralization within the Weibao deposit.

Different from the Eu and Ce anomalies in zircon, the amplitude of these anomalies in apatite is probably more strongly controlled by other factors such as the crystallization of feldspars, and the presence of other accessory phases such as monazite and fluorite (Piccoli and Candela 2002). Feldspar crystallization can concentrate Eu^{2+} from the melt (Philpotts 1970; Pun et al. 1997), whereas monazite and fluorite can concentrate Ce (Chesley et al. 1991). Therefore, it was found that the correlation between the degree of the Eu and Ce anomalies of apatite and the oxidation state of the whole rock was rather weak (Piccoli and Candela 2002). This study is such a case where apatite within barren and ore-bearing intrusions in the Weibao deposit shares similar ranges in Eu_N/Eu_N^* (0.12 to 0.26) and Ce_N/Ce_N^* ratios (1.01 to 1.12). All these observations indicate that Eu and Ce anomalies in apatite are not a good proxy of the oxidation state of magmas. Nevertheless, previous studies found that Mn concentrations in apatite appeared to be affected by the oxidation state, with high apatite Mn contents normally found in reduced magmas and lower Mn contents found in more oxidized magmas. This can be explained by the substitution of Mn^{2+} for Ca^{2+}. Apatite incorporates Mn^{2+} in preference to Mn^{3+} or Mn^{4+}, because the ionic radius and valence of Mn^{2+} are closer to Ca^{2+} than those of Mn^{3+} and Mn^{4+} (Belousova et al. 2001, 2002b; and references therein). Therefore, apatite will have elevated Mn content at low oxygen fugacity in which manganese exists principally as a divalent anion (Mn^{2+}). In the Weibao deposit, apatite within two ore-forming intrusions exhibits much lower Mn concentrations than within the barren diorite porphyry (Fig. 8e), which therefore further demonstrates the higher oxidized state (and thus higher productivity) of ore-bearing magmas in the Weibao deposit.

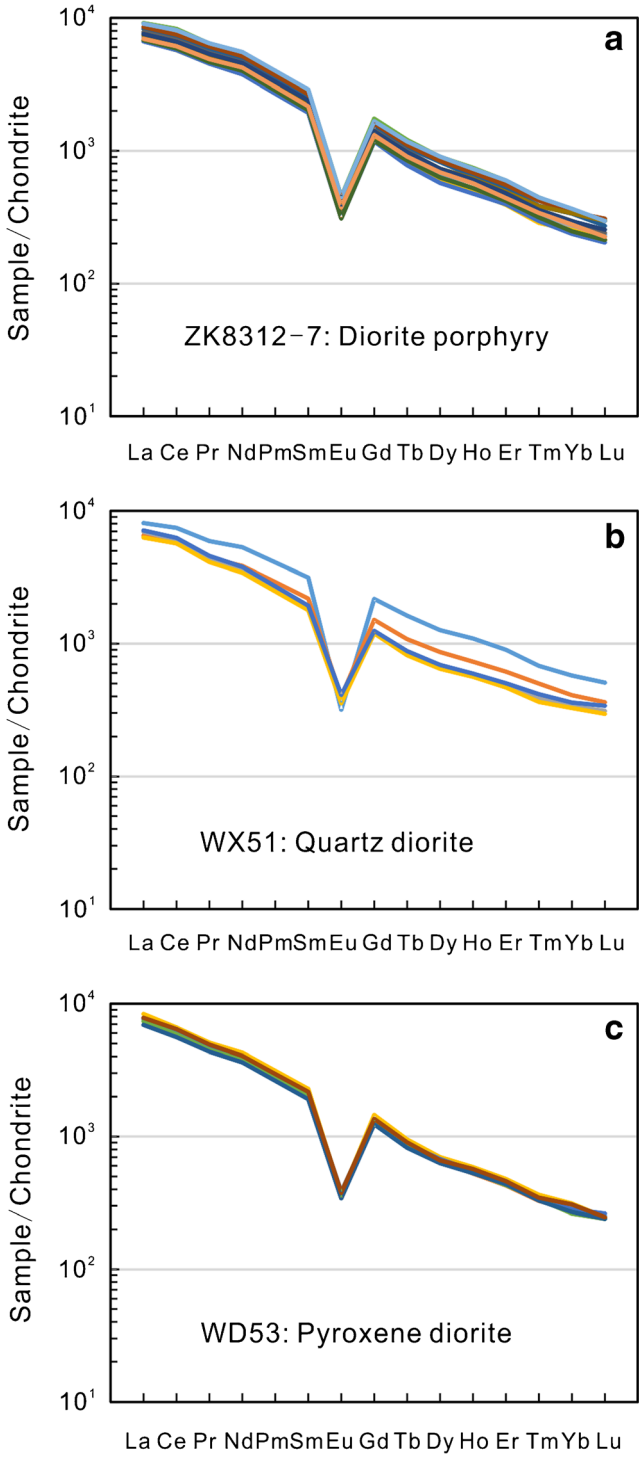

Fig. 9 **a**–**c** Chondrite-normalized REE diagrams of apatite in intrusions from the Weibao deposit

Halogen contents of magmas

Apart from the oxidation state, sthe abundance of halogens, especially fluorine and chlorine, is also of great importance for productive magmas since halogens can effectively complex and transport metals (e.g., gold, copper) (Piccoli and Candela 1994; Coulson et al. 2001; Webster et al. 2004, 2009; Mathez and Webster 2005; Pan et al. 2016). Numerous studies advocate that Cl-rich systems are more prospective for base and precious metal mineralization than Cl-barren ones, indicating that Cl contents might be a potential proxy of the fertility of magmas (e.g., Roegge et al. 1974; Piccoli and Candela 2002; Mathez and Webster 2005). Previous works demonstrated that halogen contents could be evaluated using the composition of apatite in igneous rocks (Mathez and Webster 2005; Webster et al. 2009). For mafic silicate melt containing less than ~3.8 wt% Cl (1066 to 1150 °C, 199 to 205 MPa), experiments showed that $D_{Cl}^{apatite/melt}$ (wt. fraction of Cl in apatite/Cl in melt) ≈ 0.8 and $D_F^{apatite/melt} \approx 3.4$ (Mathez and Webster 2005). The calculated Cl concentrations of the barren magma in the Weibao deposit range from 0.09 to 0.15 wt%, much lower than those of the ore-bearing magmas (ranging from 0.50 to 1.18 wt%), therefore further indicating that the two ore-bearing intrusions are more productive. In contrast, the calculated F contents of the barren and ore-bearing magmas are almost identical, ranging from 0.42 to 0.77 wt% and 0.41 to 0.72 wt%, respectively. This suggests that unlike Cl, F may not effectively control the extraction and transport of Cu, Pb, and Zn during the magmatic evolution, although it has a greater influence on the extraction and transport of Nb, Ta, Sn, and W (Thomas et al. 2004; Simons et al. 2017).

Copper productivity of magmas: Cu–Pb–Zn skarn deposits vs. porphyry Cu deposits

Contrasts in magmatic oxygen fugacity

In Fig. 6, we compare the intrusions in the Weibao deposit with those in typical porphyry Cu deposits from the literature (Ballard et al. 2002; Wang et al. 2013; Zhang et al. 2013; Wang et al. 2017; Zhao et al. 2017). It is clearly shown that the two ore-bearing intrusions in the Weibao deposit have much lower Ce^{4+}/Ce^{3+} ratios (mostly < 200) and Eu_N/Eu_N^* ratios (< 0.3) than those from porphyry copper deposits (Fig. 6), indicating that the Weibao Cu–Pb–Zn skarn deposit has much lower oxygen fugacity than porphyry Cu deposits. By examining the relationships between the oxygen fugacity and mineralization associated with Yanshanian granites in South China, Li et al. (2017b) also found that the granites related to Cu–Pb–Zn mineralization had distinctly lower oxygen fugacity than those related to porphyry Cu–(Au)–Mo mineralization. Li et al. (2008) proposed that the lower oxygen fugacity of magmas in Cu–Pb–Zn skarn deposits might result from assimilation of crustal materials. They argued that magmas generating the Cu–Pb–Zn mineralization were initially depleted in sulfur and acquired their sulfur through assimilation of crustal material, and so a relatively low oxygen fugacity could not cause significant precipitation of sulfides

in the early stages of the magmatic evolution. We do not know whether this explanation is correct, and additional data are needed to demonstrate it. Nevertheless, it is apparent that low oxygen fugacity of ore-bearing magmas for Cu–Pb–Zn skarn deposits is less favorable for Cu mineralization and, therefore, makes them less economic than porphyry Cu deposits when only copper resources are considered.

Contrasts in halogen contents of magmas

In Fig. 10, we compare the F and Cl contents of apatite from the Weibao intrusions with those from other skarn Cu–Pb–Zn and porphyry Cu deposits of the world, and a systematical variation in apatite chlorine contents is shown. It can be seen that apatite Cl contents in ore-bearing intrusions of the Weibao deposit are similar to those of other skarn Cu–Pb–Zn deposits (e.g., Baoshan and Tongshanling in SE China), but much lower than those of typical porphyry Cu deposits of the world (mostly > 0.9 wt%), although their F contents show a similar and indistinguishable range. Consequently, apatite F/Cl ratios of porphyry Cu deposits are much lower (mostly < 2) than those of Cu–Pb–Zn skarn deposits. Since Cl contents of magmas are closely related to the fertility of magmas, the above results indicate that high Cl contents of magmas may be another key factor for significant Cu mineralization.

Implications for regional mineral exploration

Previous geological studies in the Weibao deposit revealed that it was comparable to other skarn deposits in the QMB in terms of host rocks, alteration, mineralization, and igneous rock types (Gao et al. 2014b; Fang 2015; Zhou et al. 2015; Zhong et al. 2017a). In this study, we further confirm that magmatism in the Weibao deposit is similar to other skarn deposits in the QMB. This work shows that ore-bearing and barren intrusions in the Weibao deposit can be well distinguished by zircon Ce^{4+}/Ce^{3+} ratios and apatite Cl contents, with the former displaying higher zircon Ce^{4+}/Ce^{3+} ratios and apatite Cl contents. This might be a general feature of mineralized igneous rocks in the QMB, but it still awaits confirmation from data on deposits such as Kaerqueka, Hutouya in the QMB, which are in a similar geological setting. Besides, by comparing Cu–Pb–Zn skarn deposits with porphyry Cu deposits worldwide, our study shows that porphyry Cu deposits have much higher Ce^{4+}/Ce^{3+} (> 200) and Eu_N/Eu_N^* ratios (> 0.3) of zircon and higher Cl contents of apatite (> 0.9 wt%) than Cu–Pb–Zn skarn deposits. If these results are confirmed by further works, then the measurement of Ce^{4+}/Ce^{3+} and Eu_N/Eu_N^* ratios of zircon and Cl contents of apatite may provide a useful tool not only in discriminating between ore-bearing and barren intrusions at an early stage of exploration as previously suggested (e.g., Ballard et al. 2002), but also in evaluating the potential mineralization types for a certain intrusion.

Conclusions

The barren diorite porphyry and ore-bearing quartz diorite and pyroxene diorite in the Weibao deposit can be well distinguished by zircon U–Pb ages and major and/or trace element composition of zircon and apatite. The ore-bearing intrusions were emplaced in a narrow time span from 224.6 ± 2.9 to 223.3 ± 1.5 Ma which is ~ 8 m.y. later than that of the barren

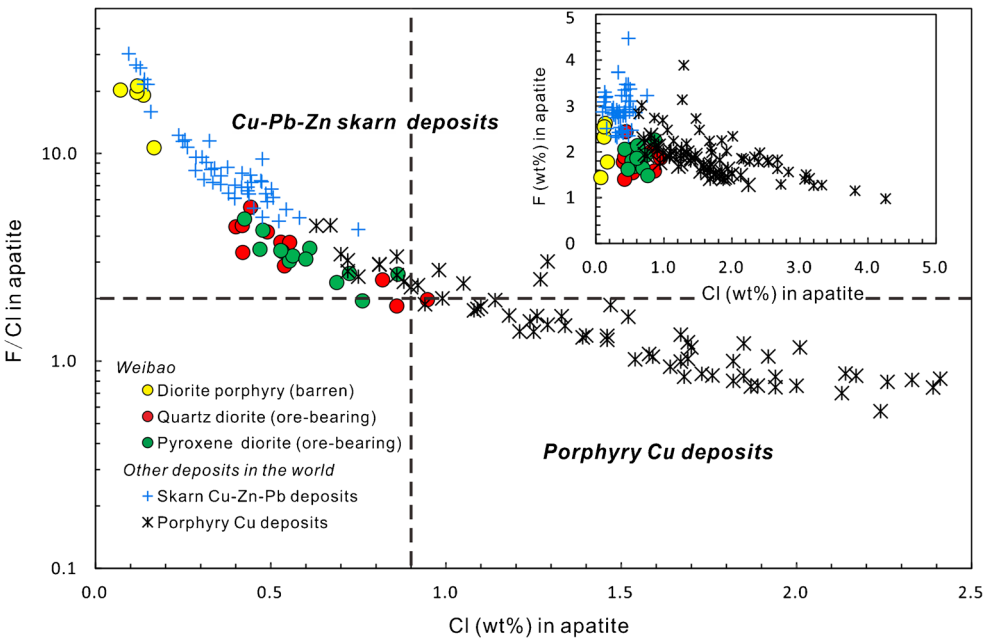

Fig. 10 Cl versus F/Cl diagram of apatite in the intrusions from Cu–Pb–Zn skarn deposits and porphyry Cu deposits. Cu–Pb–Zn skarn deposits include Weibao (this study) and Baoshan and Tongshanling in SE China (Ding et al. 2015); porphyry Cu deposits include Luoboling in SE China (Li et al. 2017a) and Lepanto-FSE, Lobo-Boneng, Black Mountain, Dizon, and Taysan in the western Luzon arc, Philippines (Imai 2002). All the intrusions are ore-forming except for the diorite porphyry from the Weibao deposit. The insert diagram shows the variations of F content with increasing Cl content of apatite

diorite porphyry (232.0 ± 2.0 Ma). They show much higher zircon Ce^{4+}/Ce^{3+} ratios and lower apatite Mn contents than the barren intrusion, indicating a much higher oxygen fugacity. Besides, they also display higher Cl contents and lower F/Cl ratios than the barren intrusion. Since both the oxidation state and halogen contents of magmas are closely related to their metal productivity, this study advocates that the quartz diorite and pyroxene diorite intrusions in the Weibao deposit were more productive than the diorite porphyry intrusion. Moreover, combined with published data, it is shown that ore-bearing intrusions of Cu–Pb–Zn skarn deposits can be distinguished from those of porphyry Cu deposits by zircon Ce^{4+}/Ce^{3+} and Eu_N/Eu_N^* ratios and apatite halogen contents. In summary, this study indicates two important applications of apatite and zircon as indicator minerals: (1) discrimination between ore-bearing and barren intrusions at an early stage of exploration and (2) evaluation of the potential mineralization types for a certain intrusion.

Acknowledgements This study was financially supported by the Geological Survey Program (Grant 1212011085528) of the China Geological Survey; the Program of High-level Geological Talents (201309) and Youth Geological Talents (201112) of the China Geological Survey; and the IGCP–592 project sponsored by IUGS–UNESCO. SZ appreciates the cooperation with the Natural History Museum (RS, AD) and the Camborne School of Mines, University of Exeter (JA) for hosting his skarn research. This is a contribution to their research on mineralized skarn systems funded by the EU Horizon 2020 project "FAME" (grant # 641650) and the Chinese Scholarship Council (fellowship to SZ). Dr. Hongying Qu, Jiannan Liu, Miao Yu, Hui Wang, and Jianhou Zhou from the CAGS are acknowledged for their assistance during the fieldwork. Special thanks are given to the Editor-in-Chief Prof. Bernd Lehmann, Associate Editor Prof. Ruizhong Hu, and anonymous reviewers for their critical and constructive reviews.

References

Baker T, Van Achterberg E, Ryan CG, Lang JR (2004) Composition and evolution of ore fluids in a magmatic-hydrothermal skarn deposit. Geology 32(2):117–120. https://doi.org/10.1130/G19950.1

Ballard JR, Palin MJ, Campbell IH (2002) Relative oxidation states of magmas inferred from Ce(IV)/Ce(III) in zircon: application to porphyry copper deposits of northern Chile. Contrib Mineral Petrol 144(3):347–364. https://doi.org/10.1007/s00410-002-0402-5

Belousova EA (2006) Zircon crystal morphology, trace element signatures and Hf isotope composition as a tool for petrogenetic modelling: examples from eastern Australian granitoids. J Petrol 47(2):329–353. https://doi.org/10.1093/petrology/egi077

Belousova EA, Walters S, Griffin WL, O'Reilly SY (2001) Trace-element signatures of apatites in granitoids from the Mt Isa Inlier, northwestern Queensland. Aust J Earth Sci 48(4):603–619. https://doi.org/10.1046/j.1440-0952.2001.00879.x

Belousova EA, Griffin W, O'Reilly SY, Fisher N (2002a) Igneous zircon: trace element composition as an indicator of source rock type. Contrib Mineral Petrol 143(5):602–622. https://doi.org/10.1007/s00410-002-0364-7

Belousova EA, Griffin WL, O'Reilly SY, Fisher NI (2002b) Apatite as an indicator mineral for mineral exploration: trace-element compositions and their relationship to host rock type. J Geochem Explor 76(1):45–69. https://doi.org/10.1016/S0375-6742(02)00204-2

Breiter K, Skoda R (2012) Vertical zonality of fractionated granite plutons reflected in zircon chemistry: the Cinovec A-type versus the Beauvoir S-type suite. Geol Carpath 63:383–398

Bruand E, Fowler M, Storey C, Darling J (2017) Apatite trace element and isotope applications to petrogenesis and provenance. Am Mineral 102(1):75–84. https://doi.org/10.2138/am-2017-5744

Burnham AD, Berry AJ (2012) An experimental study of trace element partitioning between zircon and melt as a function of oxygen fugacity. Geochim Cosmochim Acta 95:196–212. https://doi.org/10.1016/j.gca.2012.07.034

Cao M, Li G, Qin K, Seitmuratova EY, Liu Y (2012) Major and trace element characteristics of apatites in granitoids from Central Kazakhstan: implications for petrogenesis and mineralization. Resour Geol 62(1):63–83. https://doi.org/10.1111/j.1751-3928.2011.00180.x

Chen B, Zhang ZY, Geng JZ, Jian QZ, Song ZB, Zhao XF, Chen AY, Quan SC, Zhang YL, Fu YZ (2012) Zircon LA-ICP-MS U-Pb age of monzogranites in the Kaerqueka copper-polymetallic deposit of Qimantag, western Qinghai province. Geol Bull China 31:463–468 (in Chinese with English abstract)

Chesley JT, Halliday AN, Scrivener RC (1991) Samarium-neodymium direct dating of fluorite mineralization. Science 252(5008):949–951. https://doi.org/10.1126/science.252.5008.949

Coulson IM, Dipple GM, Raudsepp M (2001) Evolution of HF and HCl activity in magmatic volatiles of the gold-mineralized Emerald Lake pluton, Yukon Territory, Canada. Mineral Deposita 36(6):594–606. https://doi.org/10.1007/s001260100191

Ding T, Ma D, Lu J, Zhang R (2015) Apatite in granitoids related to polymetallic mineral deposits in southeastern Hunan Province, Shi–Hang zone, China: implications for petrogenesis and metallogenesis. Ore Geol Rev 69:104–117. https://doi.org/10.1016/j.oregeorev.2015.02.004

Fang J. (2015) Ore genesis of Weibao banded skarn lead-zinc deposit, Qimantagh area, Xinjiang, China. Dissertation, Chinese Academy of Sciences

Feng CY, Li DS, Wu ZS, Li HJ, Zhang ZY, Zhang AK, Shu XF, Su SS (2010) Major types, time-space distribution and metallogeneses of polymetallic deposits in the Qimangtage metallogenic belt, Eastern Kunlun area. Northwest Geol 43:10–17 (in Chinese with English abstract)

Feng CY, Wang XP, Shu XF, Zhang AK, Xiao Y, Liu JN, Ma SC, Li GC, Li DX (2011) Isotopic chronology of the Hutouya skarn lead-zinc polymetallic ore district in Qimantage area of Qinghai province and its geological significance. J Jilin Univ (Earth Sci Ed) 41:1806–1817 (in Chinese with English abstract)

Feng CY, Wang S, Li GC, Ma SC, Li DS (2012) Middle to Late Triassic granitoids in the Qimantage area, Qinghai Province, China: chronology, geochemistry and metallogenic significances. Acta Petrol Sin 28:665–678 (in Chinese with English abstract)

Fu Q, Xu B, Zheng Y, Yang Z, Hou Z, Huang K, Liu Y, Zhang C, Zhao L (2017) Two episodes of mineralization in the Mengya'a deposit and implications for the evolution and intensity of Pb–Zn–(Ag) mineralization in the Lhasa terrane, Tibet. Ore Geol Rev 90:877–896. https://doi.org/10.1016/j.oregeorev.2017.01.008

Gao YB, Li WY, Qian B, Li K, Li DS, He SY, Zhang ZW, Zhang JW (2014a) Geochronology, geochemistry and Hf isotopic compositions of the granitic rocks related with iron mineralization in

Yemaquan deposit, East Kunlun, NW China. Acta Petrol Sin 30: 1647–1665 (in Chinese with English abstract)

Gao YB, Li WY, Qian B, Li K, Zhang ZW, Jiang ZX, Shen DL, Wang ZH, Ye MF (2014b) Geology, fluid incluisions and S, Pb isotopic geochemistry of the Weibao Zn-Pb deposit in Qimantage, Xinjiang. J Jilin Univ (Earth Sci Ed) 44:1153–1165 (in Chinese with English abstract)

Gardiner NJ, Hawkesworth CJ, Robb LJ, Whitehouse MJ, Roberts NM, Kirkland CL, Evans NJ (2017) Contrasting granite metallogeny through the zircon record: a case study from Myanmar. Sci Rep 7(1):748. https://doi.org/10.1038/s41598-017-00832-2

Han Y, Zhang S, Pirajno F, Zhou X, Zhao G, Qü W, Liu S, Zhang J, Liang H, Yang K (2013) U–Pb and Re–Os isotopic systematics and zircon Ce^{4+}/Ce^{3+} ratios in the Shiyaogou Mo deposit in eastern Qinling, central China: insights into the oxidation state of granitoids and Mo (Au) mineralization. Ore Geol Rev 55:29–47. https://doi.org/10.1016/j.oregeorev.2013.04.006

Hou KJ, Li YH, Tian YR (2009) In situ U-Pb zircon dating using laser ablation-multi ion counting-ICP-MS. Mineral Deposits 28:481–492 (in Chinese with English abstract)

Imai A (2002) Metallogenesis of porphyry Cu deposits of the western Luzon arc, Philippines: K-Ar ages, SO_3 contents of microphenocrystic apatite and significance of intrusive rocks. Resour Geol 52(2):147–161. https://doi.org/10.1111/j.1751-3928.2002.tb00127.x

Lehmann B (1990) Metallogeny of tin. Lecture Notes in Earth Sciences. Springer Verlag, Berlin, p 32

Li SJ, Sun FY, Feng CY, Liu ZY, Zhao JW, Li YC, Wang S (2008) Geochronological study on Yazigou polymetallic deposit in Eastern Kunlun, Qinhai province. Acta Geol Sin 82:949–955 (in Chinese with English abstract)

Li QL, Li XH, Liu Y, Tang GQ, Yang JH, Zhu WG (2010) Precise U-Pb and Pb-Pb dating of Phanerozoic baddeleyite by SIMS with oxygen flooding technique. J Anal At Spectrom 25(7):1107–1113. https://doi.org/10.1039/b923444f

Li CY, Zhang H, Wang FY, Liu JQ, Sun YL, Hao XL, Li YL, Sun WD (2012) The formation of the Dabaoshan porphyry molybdenum deposit induced by slab rollback. Lithos 150:101–110. https://doi.org/10.1016/j.lithos.2012.04.001

Li CY, Hao XL, Liu JQ, Ling MX, Ding X, Zhang H, Sun WD (2017a) The formation of Luoboling porphyry Cu–Mo deposit: constraints from zircon and apatite. Lithos 272-273:291–300. https://doi.org/10.1016/j.lithos.2016.12.003

Li X, Chi G, Zhou Y, Deng T, Zhang J (2017b) Oxygen fugacity of Yanshanian granites in South China and implications for metallogeny. Ore Geol Rev 88:690–701. https://doi.org/10.1016/j.oregeorev.2017.02.002

Liang HY, Campbell IH, Allen C, Sun WD, Liu CQ, Yu HX, Xie YW, Zhang YQ (2006) Zircon Ce^{4+}/Ce^{3+} ratios and ages for Yulong ore-bearing porphyries in eastern Tibet. Mineral Deposita 41(2):152–159. https://doi.org/10.1007/s00126-005-0047-1

Liu Y, Hu Z, Gao S, Günther D, Xu J, Gao C, Chen H (2008) In situ analysis of major and trace elements of anhydrous minerals by LA-ICP-MS without applying an internal standard. Chem Geol 257(1-2):34–43. https://doi.org/10.1016/j.chemgeo.2008.08.004

Lu YJ, Loucks RR, Fiorentini M, McCuaig TC, Evans NJ, Yang Z-M, Hou Z-Q, Kirkland CL, Parra-Avila LA, Kobussen A (2016) Zircon compositions as a pathfinder for porphyry Cu±Mo±Au deposits. Econ Geol Spec Pub 19:329–347

Ludwig K (2001) Squid 1.02: a user's manual. Berkeley Geochronol Cent Spec Pub 2:15–35

Mao JW, Wang YT, Lehmann B, Yu JJ, Du AD, Mei YX, Li YT, Zang WS, Stein HJ, Zhou TF (2006) Molybdenite Re–Os and albite $^{40}Ar/^{39}Ar$ dating of Cu–Au–Mo and magnetite porphyry systems in the Yangtze River valley and metallogenic implications. Ore Geol Rev 29(3-4):307–324. https://doi.org/10.1016/j.oregeorev.2005.11.001

Mao M, Rukhlov AS, Rowins SM, Spence J, Coogan LA (2016) Apatite trace element compositions: a robust new tool for mineral exploration. Econ Geol 111(5):1187–1222. https://doi.org/10.2113/econgeo.111.5.1187

Mathez EA, Webster JD (2005) Partitioning behavior of chlorine and fluorine in the system apatite-silicate melt-fluid. Geochim Cosmochim Acta 69(5):1275–1286. https://doi.org/10.1016/j.gca.2004.08.035

Meinert LD, Dipple GM, Nicolescu S (2005) World skarn deposits. Econ Geol 100th Anniversary Volume 100:299–336

Nash WP (1984) Phosphate minerals in terrestrial igneous and metamorphic rocks. In: Nriagu JO, Moore PB (eds) Phosphate minerals, 6th edn. Springer, Verlag, pp 215–241

Niu SD, Li SR, Huizenga JM, Santosh M, Zhang DH, Zeng YJ, Li ZD, Zhao WB (2017) Zircon U-Pb geochronology and geochemistry of the intrusions associated with the Jiawula Ag-Pb-Zn deposit in the Great Xing'an Range, NE China and their implications for mineralization. Ore Geol Rev 86:35–54. https://doi.org/10.1016/j.oregeorev.2017.02.007

Pan LC, Hu RZ, Wang XS, Bi XW, Zhu JJ, Li C (2016) Apatite trace element and halogen compositions as petrogenetic-metallogenic indicators: examples from four granite plutons in the Sanjiang region, SW China. Lithos 254-255:118–130. https://doi.org/10.1016/j.lithos.2016.03.010

Patiño DAE, Roden MF, Chaumba J, Fleisher C, Yogodzinski Y (2011) Compositional variability of terrestrial mantle apatites, thermodynamic modeling of apatite volatile contents, and the halogen and water budgets of planetary mantles. Chem Geol 288:14–31. https://doi.org/10.1016/j.chemgeo.2011.05.018

Philpotts JA (1970) Redox estimation from a calculation of Eu^{2+} and Eu^{3+} concentrations in natural phases. Earth Planet Sci Lett 9(3): 257–268. https://doi.org/10.1016/0012-821X(70)90036-1

Piccoli PM, Candela PA (1994) Apatite in felsic rocks; a model for the estimation of initial halogen concentrations in the Bishop Tuff (Long Valley) and Tuolumne Intrusive Suite (Sierra Nevada Batholith) magmas. Am J Sci 294(1):92–135. https://doi.org/10.2475/ajs.294.1.92

Piccoli PM, Candela PA (2002) Apatite in igneous systems. Rev Mineral Geochem 48(1):255–292. https://doi.org/10.2138/rmg.2002.48.6

Pun A, Papike JJ, Layne GD (1997) Subsolidus REE partitioning between pyroxene and plagioclase in cumulate eucrites: an ion microprobe investigation. Geochim Cosmochim Acta 61(23):5089–5097. https://doi.org/10.1016/S0016-7037(97)00295-0

Qiao B, Pan T, Chen J (2016) Geochronology, geochemical characteristic and geological significance of granodiorite in Yemaquan iron polymetallic deposit of the East Kunlun. J Qinghai Univ (Nat Sci Ed) 34:63–73 (in Chinese with English abstract)

Qiu JT, Yu XQ, Santosh M, Zhang DH, Chen SQ, Li PJ (2013) Geochronology and magmatic oxygen fugacity of the Tongcun molybdenum deposit, northwest Zhejiang, SE China. Mineral Deposita 48(5):545–556. https://doi.org/10.1007/s00126-013-0456-5

Qu HY, Feng CY, Pei RF, He SY, Li DX, Liu JN, Wang H, Zhou JH (2015) Thermochronology of Hutouya skarn-type copper-lead-zinc polymetallic ore district in the Qimantage area, Qinghai province. Acta Geol Sin 89:498–509 (in Chinese with English abstract)

Razique A, Tosdal RM, Creaser RA (2014) Temporal evolution of the western porphyry Cu-Au systems at Reko Diq, Balochistan, western Pakistan. Econ Geol 109(7):2003–2021. https://doi.org/10.2113/econgeo.109.7.2003

Richards JP (2003) Tectono-magmatic precursors for porphyry Cu-(Mo-Au) deposit formation. Econ Geol 98(8):1515–1533. https://doi.org/10.2113/gsecongeo.98.8.1515

Roegge JS, Logsdon MJ, Young HS, Barr HB, Borcsik M, Holland HD (1974) Halogens in apatites from the Providencia area, Mexico.

Econ Geol 69(2):229–240. https://doi.org/10.2113/gsecongeo.69.2.229

Seifert W, Förster HJ, Rhede D, Tietz O, Ulrych J (2012) Mineral inclusions in placer zircon from the Ohře (Eger) Graben: new data on "strontiopyrochlore". Mineral Petrol 106(1-2):39–53. https://doi.org/10.1007/s00710-012-0221-y

Sillitoe RH (2010) Porphyry copper systems. Econ Geol 105(1):3–41. https://doi.org/10.2113/gsecongeo.105.1.3

Sillitoe RH, Bonham HF (1990) Sediment-hosted gold deposits: distal products of magmatic-hydrothermal systems. Geology 18(2):157–161. https://doi.org/10.1130/0091-7613(1990)018<0157:SHGDDP>2.3.CO;2

Simons B, Andersen JCØ, Shail RK, Jenner FE (2017) Fractionation of Li, Be, Ga, Nb, Ta, In, Sn, Sb, W and Bi in the peraluminous Early Permian Variscan granites of the Cornubian Batholith: precursor processes to magmatic-hydrothermal mineralisation. Lithos 278-281:491–512. https://doi.org/10.1016/j.lithos.2017.02.007

Sun WD, Liang HY, Ling MX, Zhan MZ, Ding X, Zhang H, Yang XY, Li YL, Ireland TR, Wei QR (2013) The link between reduced porphyry copper deposits and oxidized magmas. Geochim Cosmochim Acta 103:263–275. https://doi.org/10.1016/j.gca.2012.10.054

Sun WD, Huang RF, Li H, Hu YB, Zhang CC, Sun SJ, Zhang LP, Ding X, Li CY, Zartman RE (2015) Porphyry deposits and oxidized magmas. Ore Geol Rev 65:97–131. https://doi.org/10.1016/j.oregeorev.2014.09.004

Thomas R, Förster HJ, Rickers K, Webster JD (2004) Formation of extremely F-rich hydrous melt fractions and hydrothermal fluids during differentiation of highly evolved tin-granite magmas: a melt/fluid-inclusion study. Contrib Mineral Petrol 148:582–601

Trail D, Bruce Watson E, Tailby ND (2012) Ce and Eu anomalies in zircon as proxies for the oxidation state of magmas. Geochim Cosmochim Acta 97:70–87. https://doi.org/10.1016/j.gca.2012.08.032

Uher P, Cerny P (1998) Zircon in hercynian granitic pegmatites of the Western Carpathians, Slovakia. Geol Carpath 49:261–270

Uher P, Breiter K, Klecka M, Pivec E (1998) Zircon in highly evolved hercynian Homolka granite, Moldanubian zone, Czech Republic: indicator of magma source and petrogenesis. Geol Carpath 49:151–160

Wang S, Feng CY, Li SJ, Jiang JH, Li DS, Su BS (2009) Zircon SHRIMP U-Pb dating of granodiorite in the Kaerqueka polymetallic ore deposit, Qimantage Mountain, Qinghai Province, and its geological implications. Geol China 36:74–84 (in Chinese with English abstract)

Wang F, Liu SA, Li S, He Y (2013) Contrasting zircon Hf–O isotopes and trace elements between ore-bearing and ore-barren adakitic rocks in central-eastern China: implications for genetic relation to Cu–Au mineralization. Lithos 156:97–111

Wang Y, Chen H, Han J, Chen S, Huang B, Li C, Tian Q, Wang C, Wu J, Chen M (2017) Paleozoic tectonic evolution of the Dananhu-Tousuquan island arc belt, Eastern Tianshan: constraints from the magmatism of the Yuhai porphyry Cu deposit, Xinjiang, NW China. J Asian Earth Sci. https://doi.org/10.1016/j.jseaes.2017.05.022

Webster J, Thomas R, Förster HJ, Seltmann R, Tappen C (2004) Geochemical evolution of halogen-enriched granite magmas and mineralizing fluids of the Zinnwald tin-tungsten mining district, Erzgebirge, Germany. Mineral Deposita 39:452–472

Webster JD, Tappen CM, Mandeville CW (2009) Partitioning behavior of chlorine and fluorine in the system apatite–melt–fluid. II: felsic silicate systems at 200 MPa. Geochim Cosmochim Acta 73(3):559–581. https://doi.org/10.1016/j.gca.2008.10.034

Wittenbrink J, Lehmann B, Wiedenbeck M, Wallianos A, Dietrich A, Palacios C (2009) Boron isotope composition of melt inclusions from porphyry systems of the Central Andes: a reconnaissance study. Terra Nova 21(2):111–118. https://doi.org/10.1111/j.1365-3121.2008.00863.x

Xu QL, Sun FY, Li BL, Qian Y, Li L, Yang YQ (2014) Geochronological dating, geochemical characteristics and tectonic setting of the granite-porphyry in the Mohexiala silver polymetallic deposit, eastern Kunlun orogenic belt. Geotecton Metallog 38:421–433 (in Chinese with English abstract)

Xu L, Bi X, Hu R, Qi Y, Tang Y, Wang X, Zhu J (2016) Redox states and genesis of magmas associated with intra-continental porphyry Cu–Au mineralization within the Jinshajiang–Red River alkaline igneous belt, SW China. Ore Geol Rev 73:330–345. https://doi.org/10.1016/j.oregeorev.2015.05.007

Yu M, Feng CY, Liu HC, Li DW, Zhao YM, Li DX, Liu JN, Wang H, Zhang MH (2015) ^{40}Ar-^{39}Ar geochronology of the Galinge large skarn iron deposit in Qinghai province and geological significance. Acta Geol Sin 89:510–521 (in Chinese with English abstract)

Zhang H, Ling MX, Liu YL, Tu XL, Wang FY, Li CY, Liang HY, Yang XY, Arndt NT, Sun WD (2013) High oxygen fugacity and slab melting linked to Cu mineralization: evidence from Dexing porphyry copper deposits, southeastern China. J Geol 121(3):289–305. https://doi.org/10.1086/669975

Zhang CC, Sun WD, Wang JT, Zhang LP, Sun SJ, Wu K (2017) Oxygen fugacity and porphyry mineralization: a zircon perspective of Dexing porphyry Cu deposit, China. Geochim Cosmochim Acta 206:343–363. https://doi.org/10.1016/j.gca.2017.03.013

Zhao YM, Feng CY, Li DX, Liu JN, Xiao Y, Yu M, Ma SC (2013) Metallogenic setting and mineralization-alteration characteristics of major skarn Fe-polymetallic deposits in Qimantag area, western Qinghai Province. Mineral Deposits 32:1–19 (in Chinese with English abstract)

Zhao XB, Xue CJ, Chi GX, Mo XX, Nurtaev B, Zhang GZ (2017) Zircon and molybdenite geochronology and geochemistry of the Kalmakyr porphyry Cu–Au deposit, Almalyk district, Uzbekistan: implications for mineralization processes. Ore Geol Rev 86:807–824. https://doi.org/10.1016/j.oregeorev.2017.04.008

Zhong SH, Feng CY, Seltmann R, Li DX (2017a) Middle Devonian volcanic rocks in the Weibao Cu–Pb–Zn deposit, East Kunlun Mountains, NW China: zircon chronology and tectonic implications. Ore Geol Rev 84:309–327. https://doi.org/10.1016/j.oregeorev.2017.01.020

Zhong SH, Seltmann R, Shen P (2017b) Two different types of granitoids in the Suyunhe large porphyry Mo deposit, NW China and their genetic relationships with molybdenum mineralization. Ore Geol Rev 88:116–139. https://doi.org/10.1016/j.oregeorev.2017.04.012

Zhou JH, Feng CY, Shen DL, Li DX, Wang H, Zhang MY, Ma SC (2015) Geochronology, geochemistry and tectonic implications of granodiorite in the northwest of Weibao deposit, Xinjiang Qimantage. Acta Geol Sin 89:473–486 (in Chinese with English abstract)

Zhou JH, Feng CY, Li DX, Li GC (2016) Geological, geochemical, and geochronological characteristics of Caledonian W–Sn mineralization in the Baiganhu orefield, southeastern Xinjiang, China. Ore Geol Rev 75:125–149. https://doi.org/10.1016/j.oregeorev.2015.12.009